Wetting of Porous α-$LiAlO_2$ by Molten Carbonate

Liangjuan Gao,[1,*,z] J. Robert Selman,[2,] and Philip Nash[1]**

[1] *Mechanical, Materials, and Aerospace Engineering, Illinois Institute of Technology (IIT), Chicago, Illinois 60616, USA*
[2] *Chemical and Biological Engineering, Illinois Institute of Technology (IIT), Chicago, Illinois 60616, USA*

Cracking of α-$LiAlO_2$ matrices in molten carbonate fuel cells (MCFC) leads to reduction in the performance. It was demonstrated in this work that the mechanical strength of α-$LiAlO_2$ matrices is improved by heat-treating at 800°C under ambient gas atmosphere. The mechanical strength (2.91MPa) of the heat-treated matrix was enhanced more than 5 fold compared to the non-heat-treated matrix (0.58MPa). The porosity and crystal structure of the α-$LiAlO_2$ matrices were not changed after the heat-treatment. The wetting behavior and distribution of carbonate in the heat-treated and the non-heat-treated matrix were investigated and compared. Both non-heat-treated and heat-treated α-$LiAlO_2$ matrices were completely wetted by molten carbonate. The molten carbonate distribution was concentrated right underneath the circular region formed by the molten carbonate drop in the matrix. Non-heat-treated α-$LiAlO_2$ samples cracked as a result of the complete absorption of molten carbonate, however, the heat-treated α-$LiAlO_2$ matrices did not crack, presumably due to their enhanced mechanical strength.
 [DOI: 10.1149/2.0771805jes]

Manuscript submitted January 22, 2018; revised manuscript received March 19, 2018. Published March 30, 2018. This was Paper 1642 presented at the New Orleans, Louisiana, Meeting of the Society, May 28–June 1, 2017.

$LiAlO_2$ is widely used as the electrolyte matrix material in MCFC stacks because in the form of a porous matrix it has high capability to retain the molten electrolyte and has a good phase stability.[1] Lehmann and Hesselbarth[2] established the existence of two different phases: α- and γ-$LiAlO_2$. Lejus and Collongues[3] determined the crystallographic structure of these phases. α-$LiAlO_2$ is trigonal with a NaCl-like arrangement where each Li and Al are coordinated by 6O and show the octahedral structure. γ-$LiAlO_2$ is tetragonal where the atoms are in a tetrahedral structure with coordination number of 4. Chang and Margrave[4] have reported the existence of β-$LiAlO_2$ which has the monoclinic crystallographic structure and is meta-stable.

In the early stages of MCFC development, γ-$LiAlO_2$ was widely used as the matrix material impregnated with molten carbonate.[5] However, as the technology matured, it was found that γ-$LiAlO_2$ in contact with molten carbonate is not as stable as expected. After long-term operation of the γ-$LiAlO_2$ matrix under MCFC operating conditions, α-$LiAlO_2$ was detected in the matrix. This indicates that γ-$LiAlO_2$ transforms to α-$LiAlO_2$ in contact with the molten carbonate. The degradation in γ-$LiAlO_2$ causes a morphology change of the matrix and thereby a change of pore structure in the matrix because the density of γ-$LiAlO_2$ (2.6g/cm^3) is lower than that of α-$LiAlO_2$ (3.4g/cm^3). Tanimoto et al.[6] investigated the rate of transformation of the crystal phase of $LiAlO_2$ from the γ-phase to the α-phase under MCFC conditions in the eutectic Li_2CO_3/K_2CO_3 (62/38 mol%). Thus, 31% of the γ-$LiAlO_2$ was found to be transformed to α-$LiAlO_2$ after 15000h, and 80% after 40000h. Danek et al.[7] studied the kinetic of the α- to γ- phase transformation in $LiAlO_2$ under various conditions, including temperature, basicity of molten carbonate, as well as humidity and CO_2 partial pressure of the gas atmosphere. They found that this transformation did not take place below 700°C, which is the upper temperature limit of the MCFC operation. Moreover, it depends on the manufacturing process used for the $LiAlO_2$ material. Terada et al.[8] investigated the phase transformation process by means of in-cell tests as well as out-of-cell (gas/solid system) tests. They found that at the usual cell operating temperature (650°C), α-$LiAlO_2$ is more stable than γ-$LiAlO_2$ because α-$LiAlO_2$ has a lower solubility in molten carbonate than γ-$LiAlO_2$. They hypothesized that γ-$LiAlO_2$ dissolves in the molten carbonate and precipitates as α-$LiAlO_2$ during MCFC operation. Therefore, α-$LiAlO_2$ is gradually replacing γ-$LiAlO_2$ as the matrix material in MCFC.

The weak mechanical strength of the matrix consisting of $LiAlO_2$ particles under slight compression is a cause of failure in the long-term operation of pressurized MCFCs. Cracks in the $LiAlO_2$ matrix, almost always observed in post-test analyses after MCFC operation, cause gas cross-over between the two electrodes, which leads to "hot spots" in the matrix and eventually to decay in the cell performance. During the start-up and operation of an MCFC, the matrix experiences both mechanical and thermal stresses due to the difference in thermal expansion coefficients between the $LiAlO_2$ particles and the solid carbonate electrolyte.[9] The micro-cracks resulting from this develop further with time. Therefore, enhancement of the mechanical strength of $LiAlO_2$ to prevent cracking and ensure long term integrity of the matrix has received much attention. For example, alumina fiber has been added to the $LiAlO_2$ matrix as a crack arrestor.[10] However, Al_2O_3 (alumina) fiber has proved to be unstable in molten carbonate because of lithiation (producing $LiAlO_2$ under net volume expansion), thereby exacerbating the decay of MCFC performance. In comparison with the Al_2O_3 fiber, rod-shaped $LiAlO_2$ has shown better chemical and thermal stability and has therefore been explored extensively as a reinforcement material.[11,12] It was also found that the mechanical strength increases significantly when aluminum salts are used as the sintering aid for the $LiAlO_2$ matrix, due to the formation of necks.[13] Aluminum together with lithium carbonate was applied as the reinforcement for the matrix and proved to be economical and viable. The mismatch of the thermal expansion coefficients between the matrix and carbonate electrolyte could be controlled by adding the aluminum particles.[14] These materials have partially fulfilled the requirements for commercialization. Nevertheless, the reinforcement procedures are complicated, and some of the reinforcement additives are expensive and not stable.

The wetting behavior of the $LiAlO_2$ matrix is a very important property since it influences the active reaction area in the operation of an MCFC, and thereby the performance. Kawase et al.[15] studied the wettability of the $LiAlO_2$ in electrolyte. The contact angle value lies in the range of 10–30°. The contact angle becomes larger at high CO_2 partial pressure of the gas in contact with $LiAlO_2$ and carbonate. The contact angle appears to be nearly inversely proportional to the absolute temperature. However, the research on the wetting behavior of porous $LiAlO_2$ is limited.

In this study, a heat-treatment was applied to the porous $LiAlO_2$ matrix to enhance its mechanical strength. The effect of this

*Electrochemical Society Student Member.
**Electrochemical Society Fellow.
zE-mail: lgao7@hawk.iit.edu

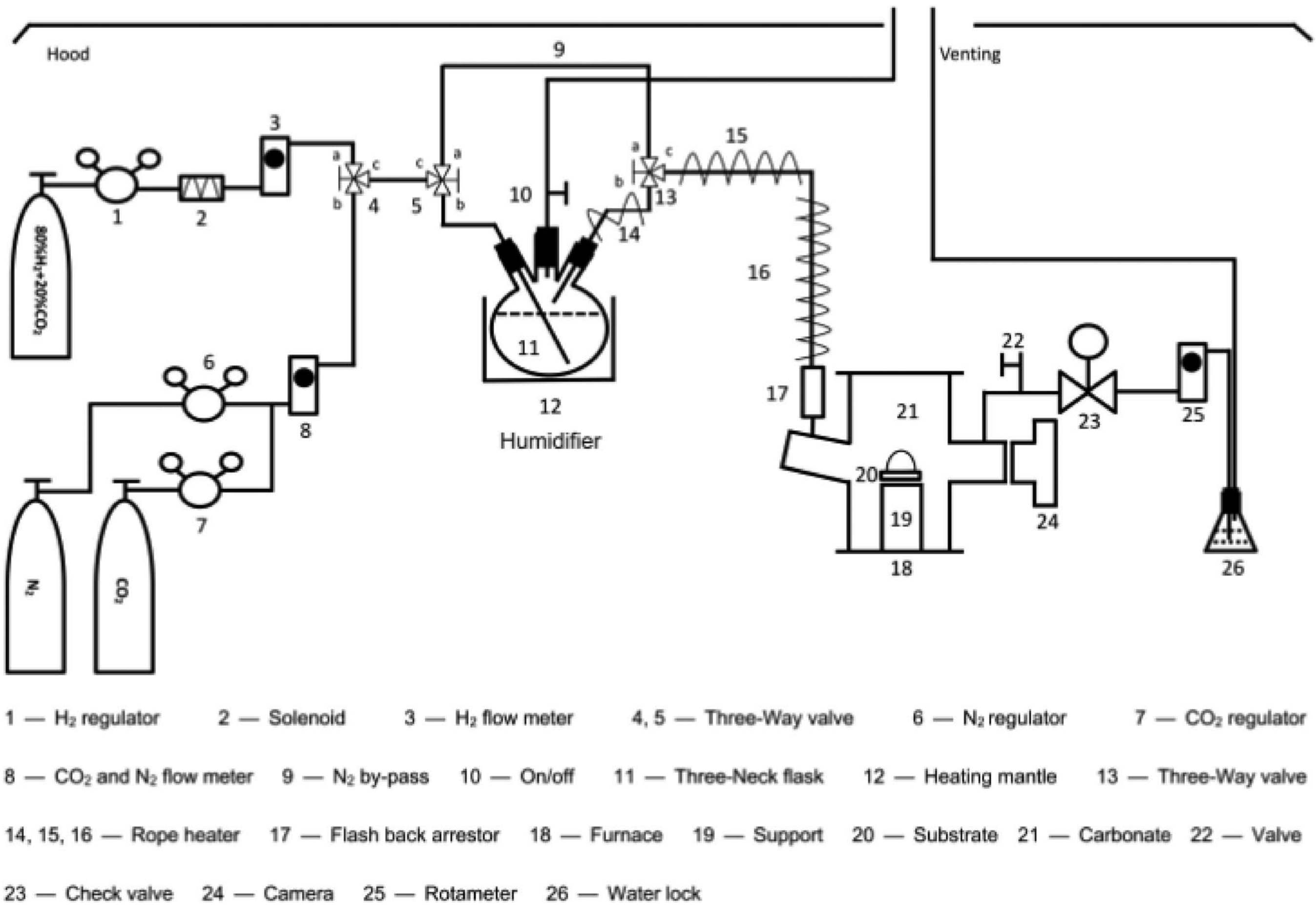

Figure 1. Schematic of experimental set up for wetting behavior investigation.

heat-treatment on wetting behavior was investigated by comparison between identical substrates with and without heat-treatment.

Experimental

Preparation and pre-treatment of the porous $LiAlO_2$ substrate.— The porous $LiAlO_2$ substrate was compacted from $LiAlO_2$ powder using a Buehler mounting press. About 2g $LiAlO_2$ powder was weighed and then poured into the 31.75mm die. A round disc substrate was made under a variety of compression stresses. The porosity, pore size distribution and pore volume of the substrate were measured by mercury intrusion porosimetry (MIP) technique, courtesy of FuelCell Energy (FCE), Inc. The porous $LiAlO_2$ substrate was heat-treated at 800°C in ambient gas atmosphere for times varying from 0h to 5h, at a heating rate of 5°C/min. Rectangular porous $LiAlO_2$ bars, of 31.75mm × 5.58mm × 12.7mm, were fabricated and heat-treated at 800°C in ambient gas atmosphere for times varying from 0h to 5h, at a heating rate of 5°C/min. The three-point bending test was applied to the as-prepared rectangular bars and the corresponding flexural strengths were obtained. The compression pressures for manufacturing the $LiAlO_2$ discs and bars were the same. Therefore, the $LiAlO_2$ discs prepared for the wetting investigation were equivalent to the bars used for bending tests.

Wetting investigation.— Fig. 1 shows the experimental set up for the wetting investigation of porous $LiAlO_2$ matrix. Briefly, it contains four main parts: (1) gas supply, (2) humidifier, (3) wetting chamber and (4) venting. The chamber is a well-sealed closed chamber which allows complete control of the atmosphere.

The sessile drop method was used to determine the contact angle. The DropSnake module in the ImageJ software was used to analyze the digital image taken of the sessile drop and obtain the contact angle values at the left-side and right-side intersection of the drop image with the substrate.[16] Generally, in the wetting chamber, the stack from bottom to top is: support, substrate and carbonate pellet (Li_2CO_3-Na_2CO_3 52:48 mol%) (as shown in Fig. 2). Upon raising the temperature, the carbonate pellet melts and forms a drop on the substrate surface. Usually the temperature is held at a steady value

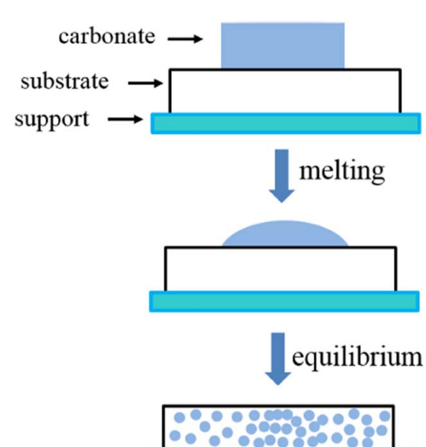

Figure 2. Schematic of the sessile drop method.

somewhat above the melting point (for example, at 580°C in a majority of cases) to allow the drop to assume equilibrium shape. The left and right contact angle values corresponding to each temperature are then measured using the ImageJ software. Since the shape of the drop was not always symmetric, in practice, the contact angle was characterized by the average of left and right contact angles.

The carbonate pellet, porous $LiAlO_2$ substrate, and thin Al_2O_3 support were stacked as shown in Fig. 2. The stack was placed on a dense ceramic support within the heating zone of the chamber. The chamber was sealed tightly and checked for leakage using a combustion detector by introducing a reducing gas mixture into the chamber. After successful testing, the furnace chamber was purged with pure N_2 gas at a flow rate of 50mL/min for 10–16h, to remove any oxygen. Reducing gas mixture at a flow rate of 50mL/min was then introduced into the furnace chamber initially at room temperature through the bypass valve for 2h while the temperature of the humidifier was brought to 45°C. Next, the temperature of the furnace chamber was raised to 80°C and held there for 20min, while the reducing gas humidified at 45°C was introduced into the furnace chamber. In order to avoid the condensation of water vapor in the humidified gas mixture the tubing from the humidifier to the furnace chamber was wrapped with a rope heater and the temperature kept at around 50°C. Then, the temperature of the furnace chamber was raised from 80°C to 400°C and held at 400°C for 1h. Thereafter, the temperature was increased from 400°C to 580°C with heating rate of 4°C/min. Telescopic images of the melting of the carbonate pellet and spreading of liquid carbonate on the porous $LiAlO_2$ surface were recorded with a Cannon digital camera. The temperature was held at 580°C for a certain time until the contact angle did not change any further under the reducing atmosphere. After that, pure CO_2 at a flow rate of 50mL/min was introduced into the furnace chamber at 580°C and the temperature held for a certain time until the contact angle did not change any further. The shape change of the drop was recorded continuously by means of a series of digital images. The videos were taken from the window mounted on the tilted tube of the furnace to record the entire process. The wetting behavior of non-heat-treated as well as heat-treated porous $LiAlO_2$ samples was investigated in this manner, and compared.

An additional experiment was carried out to investigate the competing roles of the porous $LiAlO_2$ substrate and the dense Al_2O_3 support in the spreading and absorption of molten carbonate. For this experiment, the sequence of stacking materials was, from bottom to top, dense Al_2O_3 support, carbonate pellet and porous $LiAlO_2$. The heating and purging procedures were the same as aforementioned.

Results and Discussion

Heat-treatment and mechanical strength.—Porous α-$LiAlO_2$ matrices of various porosity were made by compressing a certain amount of powder with different compression pressures. Table I lists the basic parameters of the as-prepared porous α-$LiAlO_2$ matrices. The thicknesses of the porous α-$LiAlO_2$ matrices are very close since the compression pressure could be varied only from 56.21 to 22.48MPa as the limitation of the instrument.

The porosity and pore size distribution of the porous α-$LiAlO_2$ matrices were measured by mercury intrusion porosimetry, courtesy of FCE Inc. Fig. 3 shows that the porosity of the as-prepared α-$LiAlO_2$ matrix decreases with increase of the compression pressure.

Table I. Thickness of the as-prepared porous α-$LiAlO_2$ substrates.

Sample ID.	Compression pressure (MPa)	Thickness of the substrate (mm)
1	56.21	2.06
2	44.97	2.15
3	33.73	2.46
4	22.48	2.30

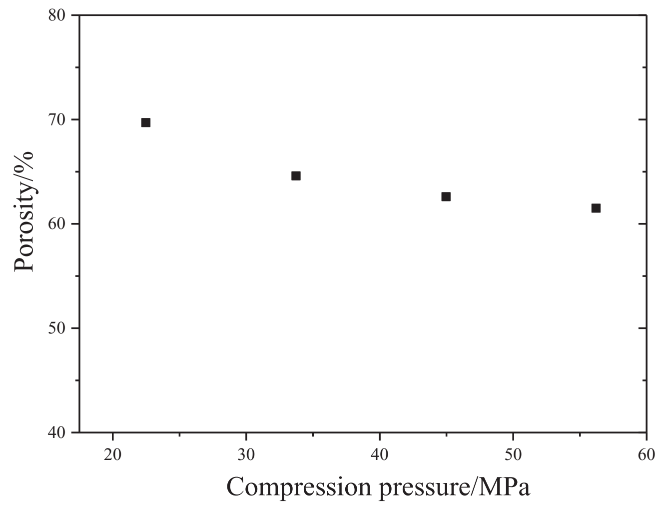

Figure 3. Porosity of as-prepared porous α-$LiAlO_2$ substrate as a function of compression pressure.

However, the decrease of porosity when the compression pressure is increased from 22MPa to 56MPa is small. The maximum applied compression pressure available was insufficient to that required for the lower porosity. Over the small range of porosities attainable in this work, it is unlikely that there is a significant change in the mechanical properties. Fig. 3 is consistent with the results in Table I.

Fig. 4 shows that the pore size distribution of the porous α-$LiAlO_2$ matrix sample is very similar in the porosity range from 61.5% to 69.7%. This range of porosity is unlikely to produce any significant effect in the mechanical properties. The average pore size of the porous α-$LiAlO_2$ matrix is about 0.07μm which is intentionally very small compared to the average pore size of the porous anodes made of nickel and nickel alloy. The average pore sizes of the as-prepared porous Ni anodes are from 0.42–3μm for the porosity range from 38.9–75.9%. The average pore sizes of the as-prepared porous Ni-Al alloy anodes are from 0.86–1.8μm for the porosity range from 26.2–35.3%. The dynamic wetting of those anodes by molten carbonate will be systematically studied in the future for comparison. It can be seen in Fig. 4 that a small peak corresponding to larger pore size also appears in the pore size distribution curve, at a porosity of 69.7%. Although this suggests a weakly bimodal pore distribution, such a pore size distribution is not favorable for the matrix because gas cross-over is not allowable in the matrix. The matrix should be

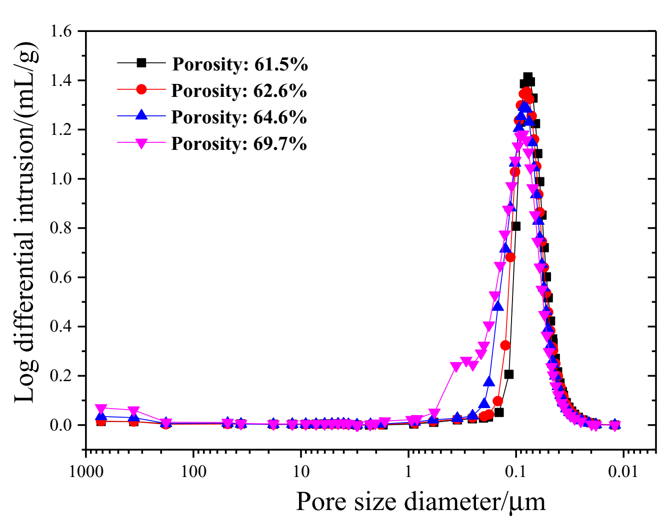

Figure 4. Distribution of pore size in the as-prepared porous α-$LiAlO_2$ matrix.

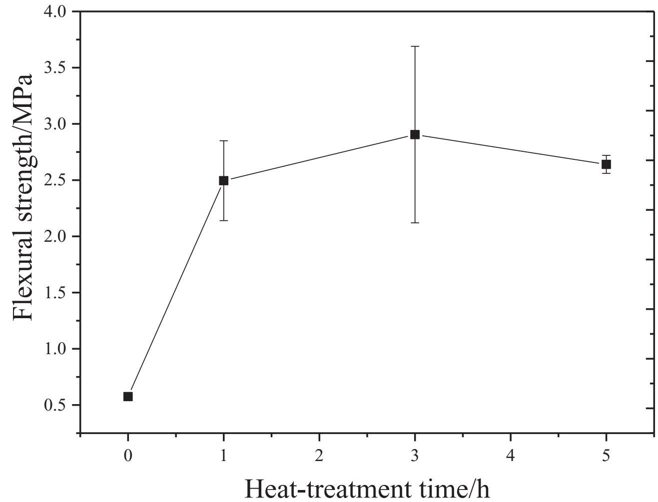

Figure 5. Variation of flexural strength of porous α-$LiAlO_2$ with heat-treatment time.

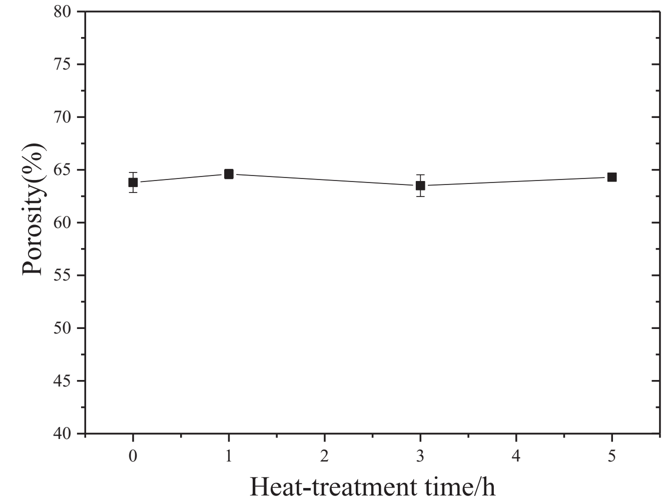

Figure 6. Dependence of porosity of as-prepared α-$LiAlO_2$ on heat-treatment duration.

completely filled with carbonate electrolyte. The porosity of α-$LiAlO_2$ matrix is usually required to be in the range of 40–70%.

The as-prepared porous α-$LiAlO_2$ matrix was heat-treated under ambient gas atmosphere at 800°C, for 1h, 3h, and 5h, respectively. The mechanical strength of the non-heat-treated and heat-treated matrices was measured by the three-point flexural bending method (Fig. 5). The flexural strength of the non-heat-treated porous α-$LiAlO_2$ matrix was found to be about 0.58MPa. By heat-treatment at 800°C for 3h the mechanical strength was found to be increased to 2.91MPa, and then slightly decreased at longer heat-treatment time to 2.64MPa. This indicates that heat-treatment at 800°C may initially enhance the mechanical strength of the porous α-$LiAlO_2$ matrix but that the effect might level off after more than 3h. It is well known that the initial step of sintering is the formation of a neck-to-neck structure which does not lead to shrinkage and we assume that this occurs in this case. Therefore, the increase in mechanical strength of the porous $LiAlO_2$ matrix after heat-treatment is likely due to neck formation.

It has been reported that the porosity of the α-$LiAlO_2$ matrix should be in the range of 40%–70%.[1] This is considered the "lifetime criterion" of the matrix porosity. If the porosity falls below 40%, the ohmic drop across the matrix will rise to values which cause an excessive decay in MCFC performance. If the porosity becomes higher than 70%, gas cross-over is facilitated. Thus the porosity of the α-$LiAlO_2$ matrix was estimated before and after the heat-treatment at 800°C. As shown in Fig. 6, the porosity of the α-$LiAlO_2$ matrix did not change significantly due to the heat-treatment and remains approximately 64%. This value is within the criterion for satisfactory operation but it is only slightly lower than the upper limit of 70%, at which gas cross-over becomes a risk.

The XRD patterns of the non-heat-treated sample matched the peaks of α-$LiAlO_2$ (as shown in Fig. 7).[17] After heat-treatment at 800°C under ambient gas atmosphere for different durations, the crystal structure of α-$LiAlO_2$ did not transform to γ-$LiAlO_2$. This indicates that α-$LiAlO_2$ is stable at 800°C under ambient gas atmosphere.

Wetting investigation.—α-$LiAlO_2$ sample was made by adding 2g α-$LiAlO_2$ powder into 31.75mm die under the compression pressure of 56.21MPa. Totally, six such samples were made. Two samples were kept as they were originally prepared without any treatments before the wetting investigation. Three samples were heat-treated under ambient gas atmosphere for 1h, 3h, and 5h, respectively. One sample was heat-treated at 580°C under reducing atmosphere for 2h and under pure CO_2 for 5h. The last sample was used to study the effect of carbonate absorption on the sample. The wetting behavior of those six samples was investigated.

As discussed earlier, the carbonate pellet sitting on the porous $LiAlO_2$ substrate (see Fig. 2) is heated slowly until it has melted completely, and the temperature is then held constant slightly above the temperature where melting is complete. This is illustrated in Fig. 8a, where the start of the constant temperature regime is set at 580°C, which is in the typical operating temperature zone of 550°C–650°C[18] for the carbonate eutectic with melting point of 500°C[19] used in this research. The sample shown in Fig. 8 was non-heat-treated porous $LiAlO_2$. During and after complete melting, the resulting liquid drop spreads on the surface of the substrate and, subsequently or simultaneously, is absorbed into the pores of the substrate. Fig. 8b shows a characteristic sequence of images recorded during the temperature increase and constant-temperature regime for a wetting experiment. The carbonate pellet, of mass 1.1g and diameter 12.7mm, placed onto the porous α-$LiAlO_2$ matrix, starts to melt at approximately 527°C and forms a dome at approximately 550°C, which appears to be a semi-fluid. Depending on circumstances melting may occur first at the top of the pellet or at the bottom contacting the top surface of the porous substrate. The carbonate continues to melt until the dome is completely liquid, forming a drop. Simultaneously the liquid carbonate spreads onto the top surface of the porous substrate. The spreading

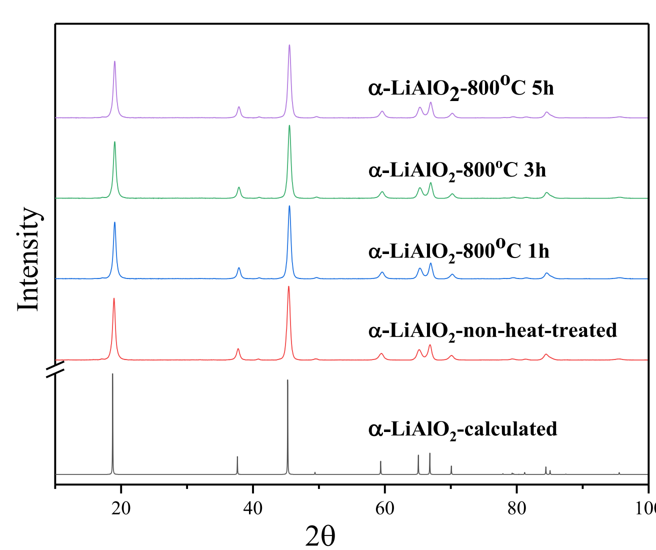

Figure 7. XRD patterns of α-$LiAlO_2$ which was calculated, not heat-treated, and heat-treated at 800°C for 1h, 3h and 5h under the ambient gas atmosphere.

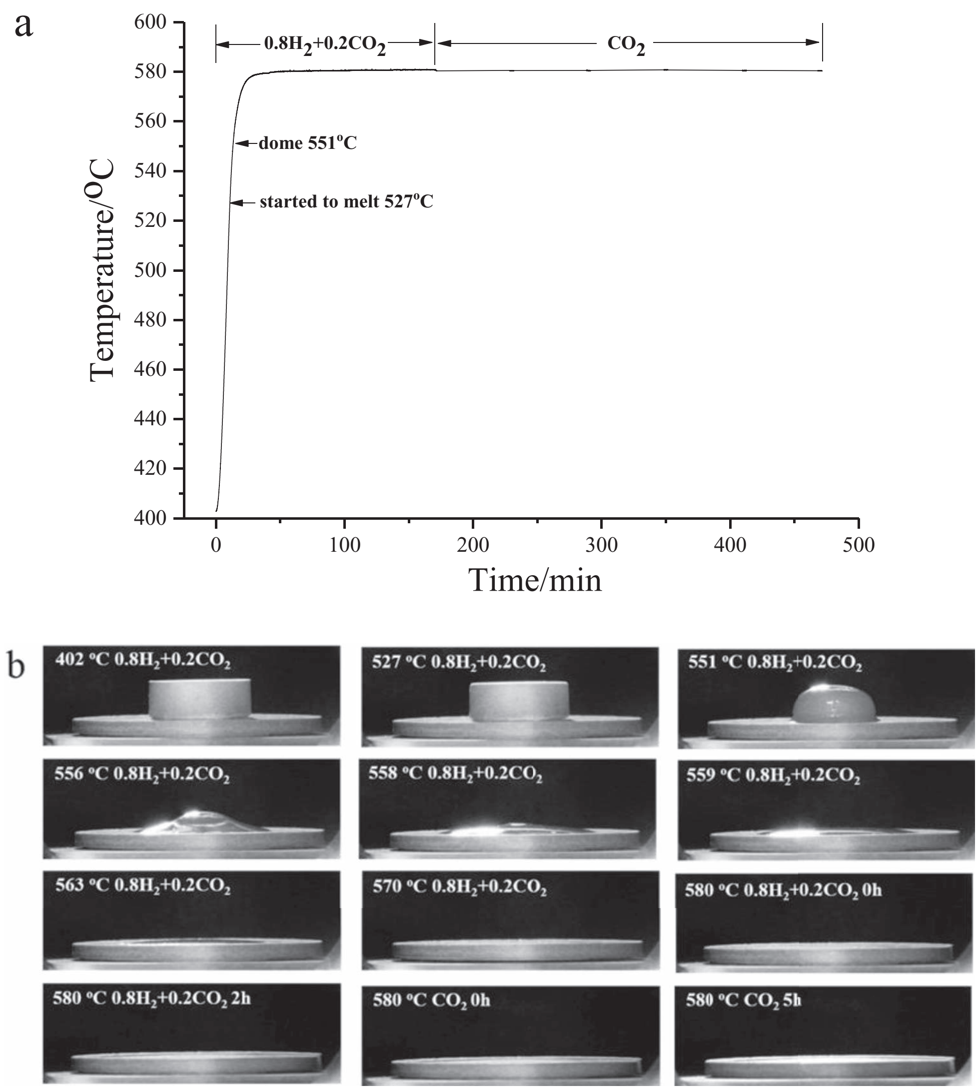

Figure 8. (a) Temperature-time graph corresponding to (b), the heating rate is 4°C/min. (b) Optical images of the melting, spreading and absorption of carbonate placed initially as a pellet onto a porous α-$LiAlO_2$ substrate. The carbonate pellet mass and diameter were 1.1g and 12.7mm, respectively. The porosity of the matrix is 64%.

process is quantified by the parameter r/R_0, that is, the ratio of the instantaneous radius of the drop, r, to the initial radius of the solid pellet, R_0, as a function of time, *t*. Usually, the drop of liquid carbonate becomes flatter as it spreads, and the radius at first increases but later decreases, indicating a loss of volume. Obviously, the drop volume decreases because penetration of molten carbonate into the pores of the substrate takes place. In most experiments the liquid drop is absorbed completely and rapidly into the porous substrate. In Fig. 8b the molten carbonate appears to be completely absorbed into the substrate before the temperature has reached the constant-temperature regime, set at 580°C.

Fig. 9 shows the contact angle and the spreading parameter r/R_0 as a function of time, for porous α-$LiAlO_2$ matrices treated under different conditions: non-heat-treated, and heat-treated under ambient gas atmosphere at 800°C for 1h, 3h, and 5h, respectively. Also shown are spreading data for a matrix heat-treated at 580°C for 2h under reducing atmosphere followed by 5h under pure CO_2 atmosphere. The dynamic contact angle and r/R_0 values are obtained under reducing atmosphere. The molten carbonate was completely absorbed into the porous α-$LiAlO_2$ before the atmosphere was switched from reducing atmosphere to pure CO_2 atmosphere. Therefore, we assume that the CO_2 did not have an effect on the wetting if it is introduced into the wetting chamber after the reducing gas. Fig. 9a shows that the contact angles in all cases reached zero after about 5min which means that the porous α-$LiAlO_2$ is completely wetted by molten carbonate regardless of the heat-treatment. The variation of contact angle with time is also barely affected, which suggests that the internal structure of the substrate (in particular, the pore size distribution) is not affected by the various heat-treatment conditions. As shown in Fig. 9b, the r/R_0 ratio increased with time to a maximum value of 1.6 at around 1.5min and then decreased rapidly to zero at around 5min in all cases.

The wetting and absorption history of the drop can therefore be divided into two stages. In the first stage, the dome of molten carbonate, initially not in mechanical and thermal equilibrium, spreads on the surface of the porous α-$LiAlO_2$ matrix while tending toward equilibrium shape at the temperature where the carbonate pellet completely melted. In the experiment, the value of r/R_0 reached a maximum when the carbonate had completely melted. Meanwhile, the contact angle decreased rapidly while the drop changed from a dome to its maximum r/R_0. Thereafter, the shrinkage of the drop took place, while the shape of the drop remained the same indicating that contact angle did not change significantly at this stage as shown in Fig. 9a. The penetration of molten carbonate from the drop into the porous α-$LiAlO_2$ matrix dominated during the shrinkage of the drop. This penetration

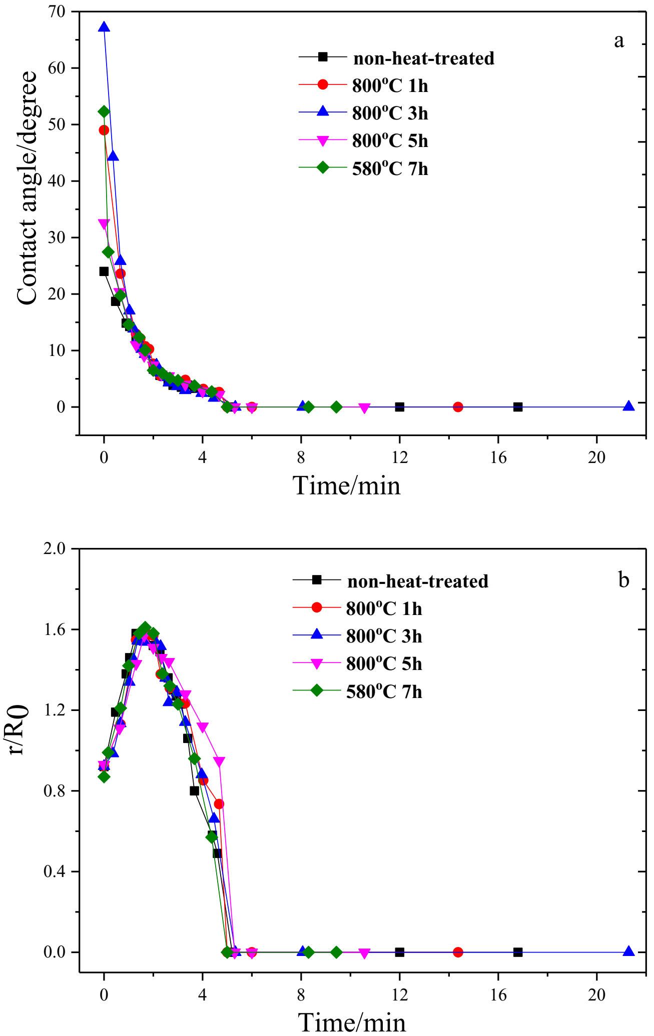

Figure 9. Variation of dynamic contact angle (θ) (a) and r/R_0 (b) with time for porous α-$LiAlO_2$ matrices heat-treated under different conditions indicated in the legends of the figures. The heat-treatments at 800°C took place under ambient gas atmosphere, for the times indicated. One matrix was heat-treated at 580°C for 7h (under a reducing atmosphere for 2h followed by 5h under pure CO_2 atmosphere).

resulted in the shrinkage of the drop base and the drop volume, and growing region of carbonate-wetted or carbonate-filled pores inside the porous α-$LiAlO_2$ matrix. When these two stages overlap, the contact angle during the overlap is found to decrease more slowly than in the first stage, but eventually goes to zero as the last molten carbonate disappears. Those two processes were consistent with the spreading and penetration processes of liquid on porous substrate reported in literature.[20]

Fig. 10 shows the absorption velocity of molten carbonate, as mass of carbonate per unit area cross-section of open pore in the substrate per unit time. It is measured that the absorption rate is close to 0.14g/min in all cases. The mass flux through the pore cross-section, is determined by dividing 0.14g/min by $A\varepsilon\rho$, where A is the pellet cross-sectional area, ε the porosity of the substrate, and ρ the density of molten carbonate at the temperature of the experiment. This yields a number expressed as $\mu m \cdot s^{-1}$, and is close to $2.43 \mu m \cdot s^{-1}$ in all cases. It indicates that the structure of all five matrices were similar regardless of heat-treatment.

A special experiment was carried out to investigate the relative wetting tendency of the porous α-$LiAlO_2$ substrate and the dense Al_2O_3 support in contact with molten carbonate. This was done by changing

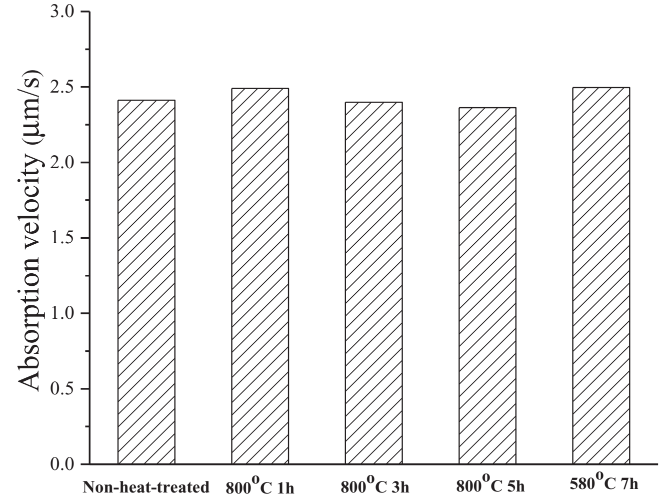

Figure 10. Variation of absorption velocity of molten carbonate with the prewetting heat-treatment of porous α-$LiAlO_2$ matrices.

the stacking sequence of the three materials (all solid at the start of the experiment) such that the carbonate pellet was in contact with the porous α-$LiAlO_2$ substrate as well as the Al_2O_3 support. The porous α-$LiAlO_2$ substrate was not heat-treated before the wetting investigation. The stacking sequence in this special experiment was therefore, from bottom to top: Al_2O_3 support, carbonate pellet, porous α-$LiAlO_2$ matrix (as shown in Fig. 11). The images recorded during the heating and constant-temperature period (Fig. 11) show that most of the molten carbonate was absorbed into the porous α-$LiAlO_2$ matrix.

As reported above for the case of a "normal" stacking sequence, the porous α-$LiAlO_2$ substrate completely absorbed the molten carbonate regardless of the heat-treatment of the porous α-$LiAlO_2$ matrix before the wetting experiment. The degree of absorption is not only determined by the intrinsic wettability of the α-$LiAlO_2$ material, but also by the pore structure inside the substrate. In the case of α-$LiAlO_2$ this probably produces a very strong capillary pressure, sufficient to drive the molten carbonate absorption to completion. Evidence of this strong capillary pressure is also observed in the post-test analysis of the substrates, as reported next.

Cracking and post-test analysis.— *Cracking analysis.*—It was observed that some of the porous α-$LiAlO_2$ matrix had developed cracks after molten carbonate was completely absorbed during the temperature increase from 400–580°C. The α-$LiAlO_2$ matrices which had not been heat-treated or which had been heat-treated at 580°C for 7h developed cracks, however, the α-$LiAlO_2$ matrices which had been heat-treated at 800°C for 1h or 3h or 5h did not develop cracks. This is illustrated in Fig. 12 which shows that the cracks occurred circumferentially along the ring marking the extent of the molten carbonate drop.

Crack development in porous α-$LiAlO_2$ matrices has been found to occur almost always during MCFC operation. There may be several reasons for crack formation. On the one hand, the mechanical strength of the non-heat-treated porous α-$LiAlO_2$ matrix is very low, about 0.58MPa as shown in Fig. 5, where the porosity was about 64%. The mechanical strength increased 5 fold after heat-treating at 800°C, however it remains quite modest compared to that of metallic sinters such as the porous nickel-alloy anode. On the other hand, the capillary pressure which drives the penetration of the molten carbonate into the pores of the α-$LiAlO_2$ matrix is relatively high compared to the force of gravity, which is the only restraint in the present experiment. According to the Young-Laplace equation, the capillary pressure p_c may be calculated by,

$$p_c = \frac{4\gamma_{LV}\cos\theta}{d} \quad [1]$$

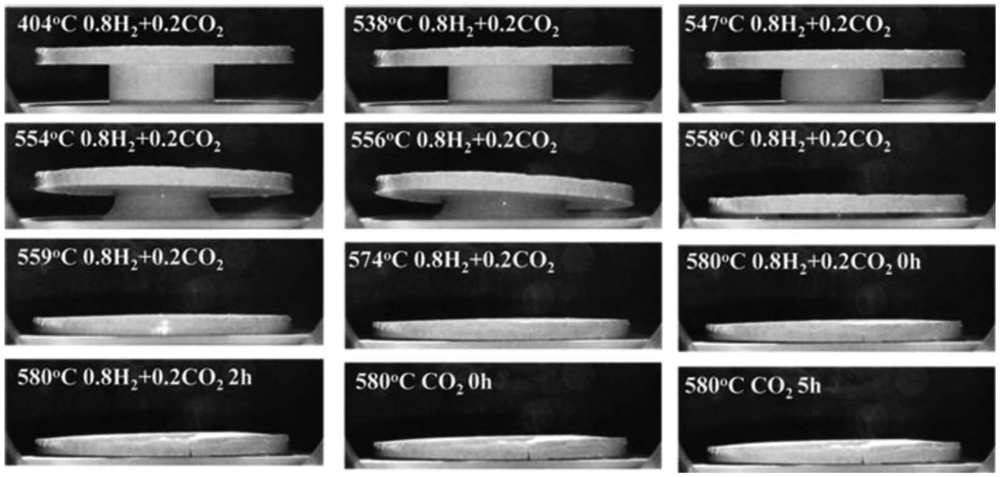

Figure 11. Wetting competition between the porous α-$LiAlO_2$ matrix and the dense Al_2O_3 support. The stacking sequence from bottom to top is: Al_2O_3, carbonate pellet, and porous α-$LiAlO_2$.

where γ_{LV} is the surface tension of molten carbonate, θ is the contact angle on the α-$LiAlO_2$ matrix, and *d* is the diameter of the pore inside the α-$LiAlO_2$ matrix. According to the literature, the surface tension of the Li-Na eutectic of molten carbonate at 580°C is about 0.244N/m.[21] The average pore diameter inside the porous α-$LiAlO_2$ matrix measured by mercury intrusion porosimetry was about 0.07μm. Therefore,

$$p_c = \frac{4\gamma_{LV}\cos\theta}{d} = 14 \times 10^6 \cos\theta \qquad [2]$$

The apparent contact angle on the surface of porous α-$LiAlO_2$ matrix was measured to be 0°. Eq. 2 then yields for the capillary pressure a value of approximately 14MPa. However on dense $LiAlO_2$, a contact angle of about 23° was measured by Kawase et al.[15] under pure CO_2 atmosphere at 570°C. Therefore, the capillary pressure calculated under this circumstance would be 13MPa, which is of the same order as the capillary pressure calculated from zero contact angle. The contact angle on $LiAlO_2$ under reducing atmosphere at 580°C is likely to be smaller than 23°, which means that the capillary pressure will be between 13MPa and 14MPa under reducing atmosphere. In any case, the capillary pressure therefore is an order of magnitude higher than the mechanical strength. In the experiments reported here it was observed that the cracking took place after the molten carbonate was completely absorbed into the porous α-$LiAlO_2$ matrix. This is consistent with the above explanation because it indicates that the driving force for the molten carbonate penetration endures even after complete absorption of the carbonate, and leads to localized breaking of the particle-to-particle bonds in the matrix, and initiation of cracks. The capillary pressure (wetting tendency of the matrix material) which drives the filling of the pores causes, in a matrix consisting of spherical particles loosely connected, a radially directed counter-force which drives the particles apart from each other. Some inter-particle bridges are thereby destroyed, and a crack starts.

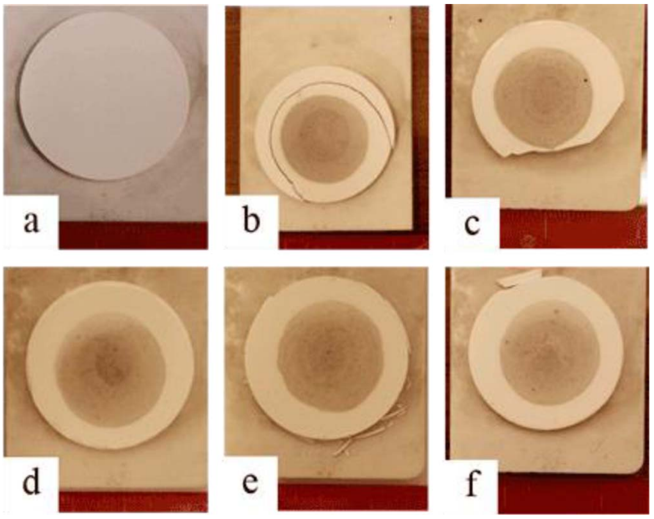

Figure 12. The optical images of the porous α-$LiAlO_2$ matrices before (a) and after (b, c, d, e, f) wetting. Before wetting, (b) had not been heat-treated, (c) heat-treated at 580°C for 7h, and (d), (e), and (f) heat-treated at 800°C for 1h, 3h, and 5h, respectively.

A third factor which may cause cracking is the difference in thermal expansion coefficients between the α-$LiAlO_2$ matrix (less than $10\times10^{-6}\text{mm}\cdot{}^\circ\text{C}^{-1}$) and the solid carbonate electrolyte (greater than $20\times10^{-6}\text{mm}\cdot{}^\circ\text{C}^{-1}$).[14] In this view, after the molten carbonate penetrates into the porous α-$LiAlO_2$ matrix, the expansion of the α-$LiAlO_2$ matrix during continued heating is less than the expansion of the molten carbonate volume, leading to stress and cracking of the α-$LiAlO_2$ matrix. However, from the video, it is clear that the actual cracking occurred shortly after the complete absorption of molten carbonate. Since there is a small temperature difference from the time carbonate is completely absorbed to the moment that cracking occurs, this indicates that the cause of the cracking is capillary pressure.

In any case, we conclude that the heat-treatment enhanced the mechanical strength of the α-$LiAlO_2$ matrix. This is favorable to prevent cracking after the penetration of molten carbonate into the porous α-$LiAlO_2$ matrix.

Post-test analysis.—It can be seen from Fig. 12 that a dark circular region is left on the top surface of the porous α-$LiAlO_2$ matrix after absorption of the molten carbonate, which seems to correspond to the actual drop diameter before it was absorbed. Around this is a less dark region. The spreading and absorption of molten carbonate on the surface and into the porous $LiAlO_2$ is schematically illustrated in Fig. 13. The schematic shows an estimate of the distribution of the molten carbonate inside the substrate. Therefore, it is very interesting to observe the morphology of the α-$LiAlO_2$ matrix and the actual distribution of the carbonate after wetting investigation by using the scanning electron microscope (SEM) and energy dispersive X-ray spectroscopy (EDS).

The cross-sectional morphology of the porous α-$LiAlO_2$ matrix after wetting investigation was characterized in the radial direction, using the SEM. It can be seen from Fig. 14 that site A, outside the dark circular region, was not fully filled with carbonate, while site B, inside the dark circular region was almost fully filled with carbonate and only

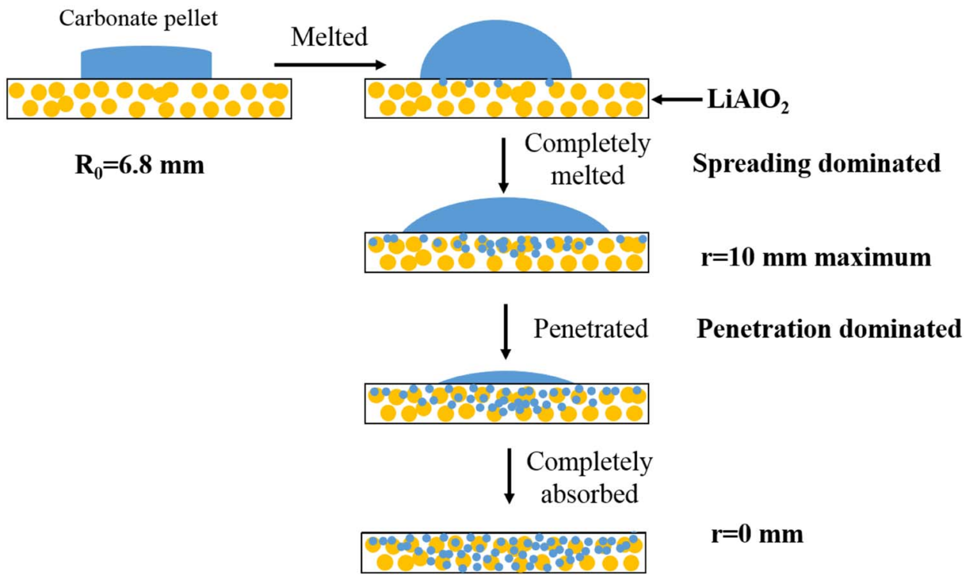

Figure 13. The total duration of carbonate behavior on and inside the porous α-$LiAlO_2$ matrix. R_0 is the initial radius of the carbonate pellet, and r is the molten carbonate drop base radius on the surface of porous α-$LiAlO_2$ matrix.

a few empty pores left. In the design of the experiment the amount of carbonate was chosen such that on average 50% of the pores inside the porous α-$LiAlO_2$ matrix would be filled by molten carbonate. After the experiment a dark circular region was observed of approximately 20mm diameter (as shown in Fig. 13). If it is assumed that this dark circular region indicates a central cylinder fully filled with molten carbonate, 78% of the molten carbonate absorbed would then be concentrated in this cylinder. The remaining 22% of the molten carbonate would therefore be distributed outside the cylindrical region. 60% of the total pores are distributed outside the central cylinder. Thus, there is a horizontal, radial component as well as a vertical, axial component of penetration into the porous substrate. The axial component obviously is strongly present immediately below the location of the sessile drop once it is formed by the melting of the pellet. But there is also a radial component which extends outward from below the original location of the sessile drop. This radial component, however, is significantly weaker than the vertical component. It can be shown, though, that this difference in orientation of the penetration velocity is not due to gravity, since the pressure due to gravity exerted by a column of penetrating carbonate melt (density $\rho = 2{,}000 kg.m^{-3}$) having a height, h, equal to the thickness (maximum vertical dimension) of the drop added to the thickness of the substrate, with h typically

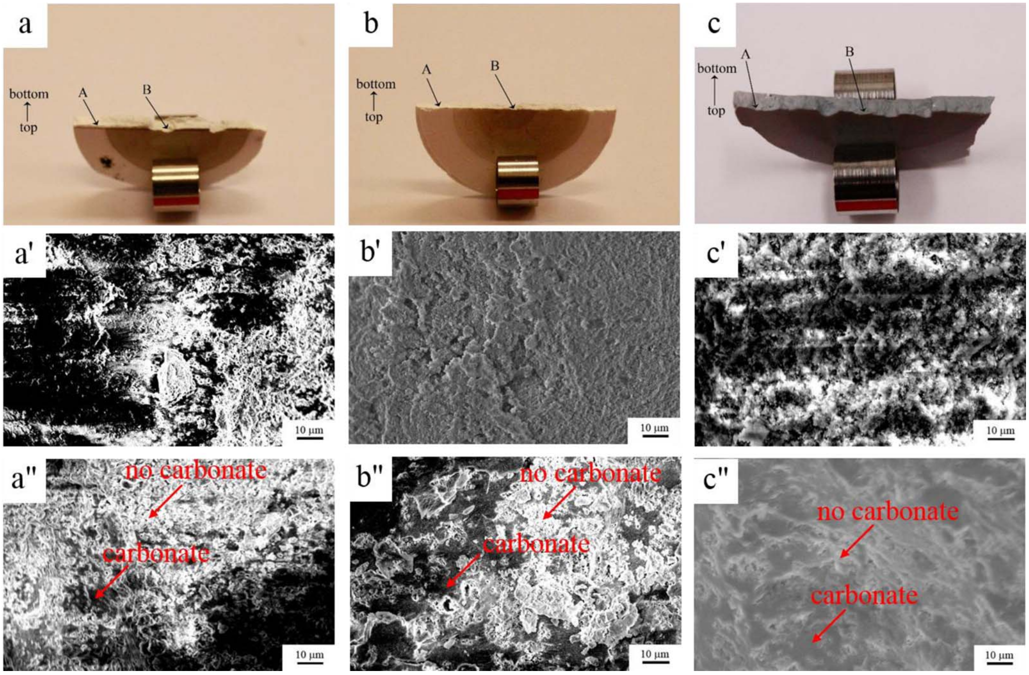

Figure 14. Optical (a, b, c) and SEM (a′, a″, b′, b″, c′, c″) images of the cross-section surface of the α-$LiAlO_2$ matrices after wetting investigation at the site inside and outside the dark central cylinder region. (a) was non-heat-treated, (a′) and (a″) are corresponding to site A and B in (a), respectively. (b) was heat-treated at 800°C for 1h, (b′) and (b″) are corresponding to site A and B in (b), respectively. (c) was heat-treated at 580°C for 7h, (c′) and (c″) are corresponding to site A and B in (c), respectively.

Table II. The overall composition at site A and B corresponding to Figs. 14a, 14b and 14c by EDS.

	Site A composition at.%				Site B composition at.%			
Sample ID.	C	O	Na	Al	C	O	Na	Al
a	8.5	66.5	8.2	16.8	9.2	66.3	8.4	16.0
b	4.6	68.2	5.3	22.0	13.7	62.9	7.6	15.9
c	5.0	67.8	5.5	21.7	17.9	62.4	6.8	12.9

0.2–1cm) is less than 200Pa. This is many orders of magnitude weaker than the capillary pressure the molten carbonate experiences in a pore of typically 0.07μm diameter completely wetted by the melt (density 2,000kg/m^3) this capillary pressure was estimated earlier to be 14MPa, see Eq. 2:

$$\rho gh = 2000\times 9.8\times 0.01 \sim 2\times 10^2 N\cdot m^{-2} << 4\gamma/d = 14\times 10^6 N\cdot m^{-2} \quad [3]$$

Consequently, the penetration of the melt into the porous substrate is driven exclusively by capillary pressure. In such a situation, the spreading of the melt is controlled by the hydrodynamic resistance presented by the porous substrate and by the geometry of the liquid phase in contact with the porous solid. In this case, and provided a practically uniform pore size distribution may be assumed, it can be argued that the extent of radial spreading to depth of axial penetration at any time, t, overall depends only on the two geometric ratios r_o/L and V/V_o. Here r_o is the radius of the sessile drop at the start of penetration, and L the thickness of the porous substrate; V is the volume of the sessile drop at the start of penetration, and V_o is the total volume of initially empty pores in the substrate. Since V_o is equal to εLA where ε is the porosity of the substrate and A is cross-sectional area (perpendicular to its thickness dimension), the two geometric parameters are evidently not independent. In particular, if L is much larger than r_o and provided enough melt volume is available for penetration, the penetration front of the liquid in the porous substrate will eventually (at large times t) become spherically symmetric with respect to the center of the initial sessile drop. The ratio of the amount of liquid absorbed in the central cylinder below the original drop and the amount absorbed in the surrounding annulus will then decrease with time independently of the parameter r_o/L and the final ratio will depend only on V/V_o. Evidently, this asymptotic state is not reached in the experiments reported here.

The overall composition of site A and B in Figs. 14a, 14b and 14c was characterized by EDS as shown in Table II. As the atomic number of Li is very low, it could not be detected by the EDS system. Sodium (Na) content was used as an indicator of the distribution of carbonate within the porous α-$LiAlO_2$ matrix. The Na content is higher at site B than at site A which is consistent with the observation reported above (concerning morphology). For the non-heat-treated sample, the difference in Na content between A and B sites is very slight. However, the difference was found to be greater for the heat-treated samples, even though it was demonstrated above that the heat-treatment did not cause significant change in the structure of the porous α-$LiAlO_2$ matrix.

An investigation to determine the particle size of α-$LiAlO_2$ after wetting experiments was carried out, by SEM analysis of samples of the substrate. As shown in Figs. 15c–15f, heat-treated samples after the wetting experiment clearly indicate coarsening of the α-$LiAlO_2$ particles. Because of the relatively short duration of the wetting tests, this can only be explained by an acceleration of the relatively slow sintering process taking place during the heat-treatment of the α-$LiAlO_2$ matrices in the absence of molten carbonate (as discussed earlier in this report). In Fig. 15 it can be seen that the spherical α-$LiAlO_2$ particles have grown and become flake-shaped. The coarsening of α-$LiAlO_2$ causes the pore size inside the porous α-$LiAlO_2$ to increase which may increase the likelihood of gas cross-over. This is not favorable for MCFC lifetime. However, the coarsening of α-$LiAlO_2$ particles was not observed in the non-heat-treated samples after wetting investigation (as shown in Figs. 15a and 15b). Neck-to-neck structure was formed in the heat-treated sample, and the presence of molten carbonate accelerated the crystal growth of heat-treated α-$LiAlO_2$. This effect is stronger for 800°C than 580°C.

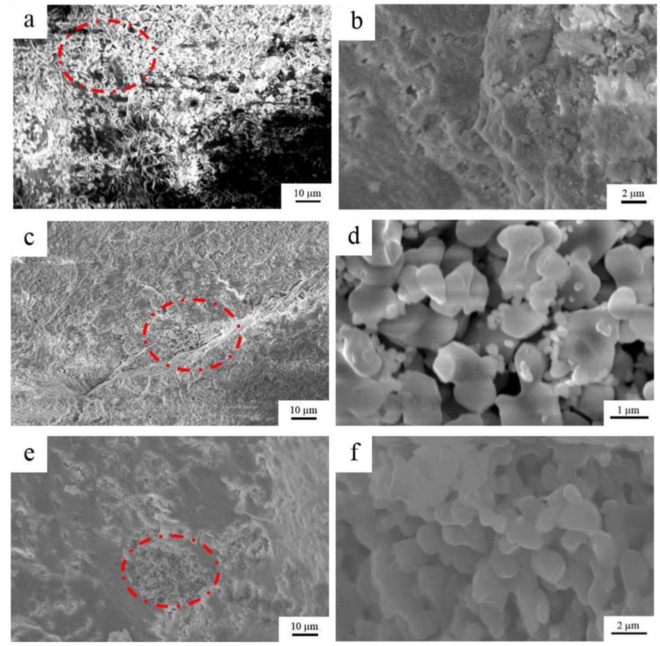

Figure 15. Coarsening of α-$LiAlO_2$ after wetting investigation: (a) non-heat-treated, (b) is the magnified image of the red circle region in (a); (c) heat-treated at 800°C for 1h, (d) is the magnified image of the red circle region in (c); (e) heat-treated at 580°C for 7h, (f) is the magnified image of the red circle region in (e).

Conclusions

Heat-treatment at 800°C under ambient gas atmosphere effectively enhances the mechanical strength of a porous α-$LiAlO_2$ matrix of the type used in MCFC operation, without causing any significant changes in the porosity of the matrix, and without causing transformation from α-$LiAlO_2$ to γ-$LiAlO_2$. The porous α-$LiAlO_2$ matrix is completely wetted by molten carbonate, regardless of the heat-treatment, and the wetting behavior of non-heat-treated and heat-treated matrices was similar. Cracking of the matrix was observed after the molten carbonate completely penetrated into a non-heat-treated α-$LiAlO_2$ matrix, or a matrix which has been heat-treated at 580°C for 7h. The crack development may be explained by the combination of poor mechanical strength of the matrix, the high capillary pressure exerted by the molten carbonate, and possibly also the thermal expansion coefficient difference between the α-$LiAlO_2$ matrix and the carbonate. Crack development was prevented by prior heat-treatment at 800°C for 3h, which substantially enhances the mechanical strength. Post-test analysis showed that the molten carbonate after penetration was mainly concentrated in the central cylindrical region observed in the porous substrate immediately below the location of the initial sessile drop, after its complete absorption. Coarsening of the α-$LiAlO_2$ particles in the matrix was observed in the presence of molten carbonate during the relatively short wetting tests, which suggests that the presence of molten carbonate accelerates the slow sintering process of the $LiAlO_2$ matrix taking place in the absence of the melt.

Acknowledgment

This study was supported by FuelCell Energy, Inc., by the program “Smart Matrix Development for Direct Carbonate Fuel Cell,” under US DOE Office of Energy Efficiency and Renewable Energy, Contract

Number: DE-EE0006606, and by the Thermal Processing Technology Center (TPTC) at IIT.

ORCID

Liangjuan Gao https://orcid.org/0000-0003-2909-4269

References

1. L. Zhou, H. Lin, and B. Yi, *Journal of power sources*, **164**, 24 (2007).
2. H. A. Lehmann and H. Hesselbarth, *Zeitschrift für anorganische und allgemeine Chemie*, **313**, 117 (1961).
3. A. Lejus and R. Collongues, *Compt. Rend*, **254**, 2005 (1962).
4. C.-H. Chang and J. L. Margrave, *Journal of the American Chemical Society*, **90**, 2020 (1968).
5. J. R. Selman, T. D. Claar, and E. Society, *Proceedings of the Symposium on Molten Carbonate Fuel Cell Technology*, Electrochemical Society (1984).
6. K. Tanimoto, M. Yanagida, T. Kojima, Y. Tamiya, H. Matsumoto, and Y. Miyazaki, *Journal of power sources*, **72**, 77 (1998).
7. V. Danek, M. Tarniowy, and L. Suski, *Journal of materials science*, **39**, 2429 (2004).
8. S. Terada, K. Higaki, I. Nagashima, and Y. Ito, *Journal of Power Sources*, **83**, 227 (1999).
9. C. L. Bushnell, L. J. Bregoli, and C. R. Schroll, *Electrolyte matrix for molten carbonate fuel cells*, in, Google Patents (1982).
10. J. Selman, H. Maru, D. Shores, and I. Uchida, Proceedings of the 2nd symposium on molten carbonate fuel cell technology, in, Pennington, NJ (USA); The Electrochemical Society (1990).
11. S. Hyun, S. Cho, J. Cho, D. Ko, and S. Hong, *Journal of materials science*, **36**, 441 (2001).
12. S.-D. Kim, S.-H. Hyun, T. H. Lim, and S. A. Hong, *Journal of Power Sources*, **137**, 24 (2004).
13. I. Lee, W. Kim, Y. Moon, H. Lim, and D. Lee, *Journal of power sources*, **101**, 90 (2001).
14. J.-J. Lee, H.-J. Choi, S.-H. Hyun, and H.-C. Im, *Journal of Power Sources*, **179**, 504 (2008).
15. M. Kawase, K. Asano, H. Murata, Y. Mugikura, T. Watanabe, and Y. Ito, *Journal of applied electrochemistry*, **32**, 185 (2002).
16. A. F. Stalder, G. Kulik, D. Sage, L. Barbieri, and P. Hoffmann, *Colloids and Surfaces A: Physicochemical and Engineering Aspects*, **286**, 92 (2006).
17. M. Marezio and J. P. Remeika, *The Journal of Chemical Physics*, **44**, 3143 (1966).
18. L. Chen and C.-Y. Yuh, *Acta Metallurgica Sinica (English Letters)*, **30**, 289 (2017).
19. G. J. JANZ and M. R. LORENZ, *Journal of chemical and Engineering data*, **6**, 321 (1961).
20. V. Starov, S. Zhdanov, S. Kosvintsev, V. Sobolev, and M. Velarde, *Advances in Colloid and Interface Science*, **104**, 123 (2003).
21. G. J. Janz, C. B. Allen, N. P. Bansal, R. M. Murphy, and R. P. T. Tomkins, *Physical properties data compilations relevant to energy storage. II. Molten salts: data on single and multi-component salt systems*, in, United States (1979).